Published in final edited form as:
Nat Microbiol. 2019 June 05; 4(9): 1545–1557. doi:10.1038/s41564-019-0479-5.

DNA-uptake pili of *Vibrio cholerae* are required for chitin colonisation and capable of kin recognition via sequence-specific self-interaction

David. W. Adams[*], **Sandrine Stutzmann**, **Candice Stoudmann**, **Melanie Blokesch**[*]
Laboratory of Molecular Microbiology, Global Health Institute, School of Life Sciences, Station 19, EPFL-SV-UPBLO, Swiss Federal Institute of Technology Lausanne (Ecole Polytechnique Fédérale de Lausanne; EPFL), CH-1015 Lausanne, Switzerland

Abstract

How bacteria colonise surfaces and how they distinguish the individuals around them are fundamental biological questions. Type IV pili are a widespread and multi-purpose class of cell surface polymers. Here we directly visualise the DNA-uptake pilus of *Vibrio cholerae*, which is produced specifically during growth upon its natural habitat - chitinous surfaces. As predicted, these pili are highly dynamic and retract prior to DNA-uptake during competence for natural transformation. Interestingly, DNA-uptake pili can also self-interact to mediate auto-aggregation. This capability is conserved in disease-causing pandemic strains, which typically encode the same major pilin subunit, PilA. Unexpectedly, however, we discovered that extensive strain-to-strain variability in PilA, present in environmental isolates, creates a set of highly specific interactions, enabling cells producing pili composed of different PilA subunits to distinguish between one another. We go on to show that DNA-uptake pili bind to chitinous surfaces, are required for chitin colonisation under flow, and that pili capable of self-interaction connect cells on chitin within dense pili networks. Our results suggest a model whereby DNA-uptake pili function to promote inter-bacterial interactions during surface colonisation. Moreover, they provide evidence that type IV pili could offer a simple and potentially widespread mechanism for bacterial kin recognition.

Keywords

Auto-aggregation; DNA uptake; natural transformation; pilus dynamics; type IV pilus; *Vibrio cholerae*

[*]Correspondence to David W. Adams or Melanie Blokesch: david.adams@epfl.ch or melanie.blokesch@epfl.ch.

Data availability
The data that support the findings of this study are available from the corresponding authors upon request.

Author contributions
Conception, design and analysis: D.W.A and M.B. Performed research: D.W.A, S.S, C.S and M.B. Wrote the manuscript: D.W.A and M.B.

Competing interests
The authors declare no competing interests.

Europe PMC Funders Author Manuscripts

Introduction

How bacteria physically sense and interact with their environment is a fundamental problem in biology. Type IV pili (T4P) are cell surface polymers ideally suited to this task1. Composed of a single major pilin and assembled by widely distributed and conserved machinery, T4P exhibit extensive functional versatility, with roles in motility, DNA-uptake, surface sensing and adhesion2,3. Consequently, T4P are critical virulence factors for numerous important human pathogens including *Vibrio cholerae*, which causes the pandemic diarrhoeal disease cholera. In Gram-negative bacteria pilins are processed at the inner-membrane, extracted by the assembly machinery and polymerised into a helical pilus fibre that exits the cell surface through a gated outer-membrane pore; the secretin4–7. A key feature of T4P is their ability to undergo dynamic cycles of extension and retraction8,9, powered by the action of dedicated extension (*e.g.* PilB) and retraction (*e.g.* PilT) ATPases, which either add or liberate pilin subunits at the base10,11. These dynamics are essential for many T4P functions *e.g.* twitching-motility8,9. Thus, understanding how T4P function may yield insights valuable for understanding mechanisms of environmental survival and pathogenesis.

Despite their multifunctional potential, pandemic *V. cholerae* strains typically encode three distinct T4P systems – two of which are well characterised. First, toxin co-regulated pili (TCP) serve a dual role as both a receptor for CTXφ bacteriophage12, which carries the cholera toxin genes, and as the primary human colonisation factor with multiple essential roles in infection involving adhesion and auto-aggregation on the intestinal cell surface13–15. Second, Mannose-sensitive haemagglutinin (MSHA) pili are involved in surface sensing and attachment and thus, are important in the initiation of biofilm formation16–20. Third, in its natural aquatic environment *V. cholerae* often associates with chitinous surfaces21, which are nutritious, foster biofilm formation and likely play a role in environmental dissemination and transmission to humans in cholera endemic regions22–24. Chitin utilisation triggers competence for natural transformation25, a widely used mode of horizontal gene transfer that allows bacteria to take up DNA from their environment, and which can thus, foster rapid bacterial evolution26. This requires the production of the Chitin-Regulated (ChiRP) or DNA-uptake pilus24,25. Importantly, in strains representative of the on-going 7th cholera pandemic such as A1552, the O1 El Tor clinical isolate used throughout this work, only MSHA pili are produced constitutively under laboratory conditions.

We previously showed DNA-uptake pili form *bona fide* pili composed of the major subunit PilA and that transformation was dependent on the presumed retraction ATPase PilT27. However, the pilus itself is not sufficient for transformation and requires the concerted action of a periplasmic DNA-binding protein, ComEA27,28. Upon receipt of transforming DNA ComEA switches from a diffuse to focal localisation28,29. These findings, together with work in other organisms, led to a model in which pilus retraction facilitates DNA entry into the periplasm30, wherein ComEA acts as ‘ratchet’ to pull in the remaining DNA28. Subsequently, DNA transport across the inner-membrane occurs via a spatially coupled channel, ComEC29. Though this model is well supported by genetic experiments27 and the similarly combined action of T4P and ComEA in other organisms31,32, direct evidence remained lacking.

Here, using a recently validated cysteine-labelling approach33, we show that, as predicted, DNA-uptake pili are highly dynamic and that these dynamics are PilT-dependent. Unexpectedly, DNA-uptake pili can self-interact, resulting in auto-aggregation. Remarkably, specific interactions between divergent PilA subunits allow pili composed of different PilA subunits to distinguish between one-another, enabling a simple mechanism for kin recognition.

Results

Direct observation of pilus dynamics by cysteine labelling

We first identified and validated a fully-transformable PilA cysteine variant (PilA[S67C]), using a chitin-independent transformation system in which competence induction is arabinose-inducible34 (Tn*tfoX*; see methods) (Fig. 1A, B and Supplementary Figs. 1, 2A-C). When stained using a thiol-reactive dye, competent cells producing PilA[S67C] exhibited visible pili (Fig. 1C). On average 27±3% of cells were piliated, with most displaying 1 or 2 pili per cell (Fig. 1H and I). Pili length clustered around 1-2 μm, although pili up to 10 μm in length were also observed (Fig. 1J). Intriguingly, detached pili frequently appeared to self-interact, forming large structures composed of networks of pili (Supplementary Fig. 3A). When examined by time-lapse microscopy cells exhibited rapid pilus dynamics, with multiple assembly and retraction events immediately apparent (Fig. 1K; Video 1-4). Indeed, within the 1 minute time-frame studied 66±3% of cells exhibited pili, with most cells producing 1-2 pili per minute (Fig. 1M). Notably, some cells were even more dynamic, elaborating ≥5 pili per minute. Consistent with this dynamic behaviour, and in support of the hypothesis that pilus retraction precedes DNA-uptake, it was possible to concurrently visualise pilus retraction followed by DNA-uptake, by monitoring the re-localisation of ComEA-mCherry, which occurs upon DNA-binding in the periplasm (Supplementary Fig. 4; Video 5).

As expected, deletion of components required for pilus assembly (*e.g.* the assembly ATPase PilB or the secretin PilQ) abolished piliation (Fig. 1D and E). However, despite the absence of obvious pili the cell body still stained. Control experiments indicate this results from non-specific dye-uptake and retention by the inner-membrane pool of PilA[S67C] (Supplementary Fig. 2D). Like other species, *V. cholerae* encodes two potential retraction ATPases, PilT and PilU. Deletion of *pilU* did not affect piliation (Fig. 1F, H-I), consistent with its dispensability for transformation27. In contrast, cells lacking the presumed retraction ATPase PilT were hyper-piliated, with essentially all cells displaying multiple static pili (Fig. 1G-I and L; Video 6-7). Taken together with the dynamics described above, these data are consistent with the presence of multiple assembly complexes scattered across the cell, as previously predicted based on the mobility of PilB and the presence of multiple PilQ foci27. This might normally serve to facilitate rapid switching of pilus location or else might reflect a need to produce multiple pili under certain conditions. Unexpectedly, retraction-deficient Δ*pilT* cells were often grouped into small clusters within dense networks of pili as well as occasionally large aggregates of pili-encased cells (Supplementary Fig. 3B-C). Indeed, when grown in liquid culture cells appeared to auto-aggregate.

Competent cells auto-aggregate in the absence of pilus retraction

Strikingly, aggregation occurred specifically in competence-induced cells lacking *pilT* (Fig. 2A-C), with the formation of large, multi-layered spherical aggregates on the order of 25-100 μm, which progress to form macroscopic aggregates that rapidly sediment (Fig. 2B, +Ara). Quantification of the ratio of cells remaining in solution to those in the settled aggregates (Fig. 2D) revealed that upon competence induction, ≥90% of the retraction-deficient cells were present in aggregates (Fig. 2D). Notably, strains producing the PilA[S67C] variant used for labelling behave similarly (Fig. 1B). Importantly, complementation of Δ*pilT* was sufficient to fully restore the ~1000-fold transformation defect and abolished the aggregation phenotype (Fig. 2D and E). Complementation also fully counteracted the enhanced motility phenotype of Δ*pilT* (Supplementary Fig. 5), which occurs due to loss of function in the adhesive MSHA pilus, in agreement with the established shared role of PilT in MSHA pilus function20,35. Finally, time-course experiments indicated that aggregation occurs abruptly, via the accretion of smaller aggregates (Supplementary Fig. 6), and that these aggregates remain stable and did not disperse, even after prolonged overnight culture.

Aggregates form via pilus-pilus interactions

The data so far suggest that hyper-piliated cells auto-aggregate via their DNA-uptake pili. Indeed, deletions affecting DNA-uptake pilus assembly (*pilQ* and *pilA*) were sufficient to abolish aggregation (Fig. 2F). In contrast, TCP (*tcpA*) and MSHA (*mshA*) pili, the *Vibrio* polysaccharide matrix (*vpsA*) required for biofilm formation36 or the flagellum (*flaA*), were dispensable, both individually and in combination (Fig. 2F). Similarly, an array of additional genes responsible for cell surface features were also dispensable (Supplementary Fig. 7A). Moreover, an ‘orphan’ type IV pilin *VC0502* encoded on the *Vibrio* seventh pandemic island II, did not affect transformation, aggregation or motility (Supplementary Fig. 7B-D). Additionally growth under high salt conditions (LB-S), which better reflects the natural aquatic environment of *Vibrio sp.* (Supplementary Fig. 7E) or in the presence of BSA, which was reported to disrupt pilus-pilus interactions in *Neisseria gonorrhoeae*37, also had no effect (Supplementary Fig. 7E). Curiously, however, the strength of the aggregation phenotype is sensitive to divalent cation concentration (Supplementary Fig. 7F), though the significance of this result remains unclear. Finally, co-culture experiments using GFP -/+ cells (Fig. 2G-I) revealed that only when both cells are hyper-piliated do they form well-mixed aggregates, indicating that aggregation occurs via direct pilus-pilus interactions between DNA-uptake pili. And, consistent with the results above, MSHA pili do not mediate auto-aggregation, even when artificially up-regulated (Supplementary Fig. 8).

PilA from pandemic strains is sufficient for aggregation in a non-pandemic strain

Deletion of *pilT* in a set of six additional 7th pandemic O1 El Tor isolates revealed that the ability to auto-aggregate is conserved among pandemic strains (Fig. 3A). Surprisingly, N16961 did not aggregate unless its well-characterised *hapR* frame-shift mutation38, which renders it quorum-sensing (QS) defective, was first repaired (Fig. 3A). Since the genes required for pilus assembly are not QS-regulated34 this suggests that there may be an additional layer of post-transcriptional control.

PilA varies considerably between environmental strains of *V. cholerae*39, whereas most clinical isolates encode an identical PilA. Interesting exceptions are the toxigenic O37-serogroup strains V52 and ATCC25872, which were responsible for limited epidemics in the 1960's40,41. They are thought to derive from a pandemic O1-classical progenitor via serogroup-conversion42. However, they both encode the same PilA that is only 50% identical to that typical of pandemic strains (Supplementary Fig. 9). Since ATCC25872, but not V52, is QS-proficient we used it to investigate the functionality of this atypical PilA. Indeed, the transformability of ATCC25872 is comparable to that of A1552, and is PilT-dependent (Fig. 3B). In contrast, however, cells lacking *pilT* did not auto-aggregate and were excluded from aggregates formed by A1552 (Fig. 3C-E, H-I).

Since the other components required for pilus assembly are all highly conserved, we tested whether PilA itself was responsible for this phenotype by exchanging the endogenous *pilA* for that of A1552 (ATCC25872-*pilA*ex). As expected, ATCC25872-*pilA*ex was fully transformable (Fig. 3B). Importantly, however, competence-induced cells of this strain lacking *pilT* were now able to auto-aggregate, albeit at lower levels than in A1552 (Fig. 3C, F-G), and intermix within aggregates formed by A1552 (Fig. 3J-K).

PilA variability governs auto-aggregation and enables kin-recognition

The results above suggest that the ability to aggregate is dependent on the particular PilA variant carried. Indeed, BLAST analyses of 647 *V. cholerae* genomes deposited in NCBI indicated that PilA exhibits extensive variation, whereas the other proteins encoded within its operon, as well as those from neighbouring genes, are all highly conserved (Supplementary Fig. 10). Of the 636 intact *pilA* genes identified, the majority (492/636) encode an 'A1552-type' PilA, likely due to over-representation of patient-derived pandemic strains in the database. Next, we extracted the unique PilA coding sequences (56/636) (Supplementary Fig. 11A) and combined them with those of an in-house collection of various environmental and patient isolates. The resulting phylogenetic tree consists of around 12 distinct groups and was used to sample PilA diversity (Fig. 4A). As expected, the N-terminal domains, required for membrane trafficking and pre-pilin peptidase recognition, and that goes on to form the long structural alpha helix (α1), are well conserved. In contrast, apart from a few clusters of key conserved residues, including the characteristic disulphide-bonded region, the C-terminal domains are highly variable (Supplementary Fig. 11A-B).

To test how PilA variability affects pilus function but avoid the potential problems of working in various strain backgrounds, we inserted new *pilA* alleles at the native *pilA* locus in strain A1552, using a short (30 bp) duplication of the 3' end of the original *pilA* to maintain any downstream-regulation. We validated this *pilA* replacement (*pilA*rep) approach using A1552-PilA (*i.e.* Tn*tfoX*, *pilA*rep[A1552]), which is fully transformable, and in cells lacking *pilT* fully auto-aggregates (Fig. 4B-C). We then tested 16 different PilA sequences from across the tree (Fig. 4A and Supplementary Fig. 11B). Interestingly, all supported transformation equally (Fig. 4B). In contrast, the ability to aggregate varied depending on the particular PilA. Indeed, in retraction-deficient cells 9/16 PilAs could auto-aggregate, though *pilA*rep[DRC186-4] was intermediate, whereas 7/16 did not detectably aggregate (Fig. 4A and C).

Given that aggregation occurs via direct pilus-pilus interactions we hypothesised that the variability between the different aggregation-proficient PilA might allow pili composed of different PilA to distinguish between one-another. To test this idea we again used a co-culture approach, using strains -/+ constitutive GFP production, and examined all possible combinations (Fig. 4D). As expected, cells producing pili composed of an identical PilA always exhibited uniform mixing (Fig. 4D-E). Remarkably, however, in 41/45 possible unique combinations the interactions between different pili were highly specific (Fig. 4D). Indeed, cells of these strains aggregated in a pilin-specific manner, preferentially forming aggregates with cells producing pili composed of the same PilA, resulting in aggregates that were either almost exclusively fluorescent or non-fluorescent (Fig. 4F). In 4/45 cases a partial cross-interaction was observed, resulting in an intermediate mixing phenotype, with aggregates composed of smaller but still segregated groups of cells (Fig. 4D and G). Overall these data indicate that pili composed of different PilA are able to discriminate between one-another, likely via specific PilA-PilA interactions. Moreover, these data demonstrate that PilA variability not only determines the ability to aggregate, but also provides a mechanism for kin-recognition.

Finally, upon virulence induction, TCP mediate auto-aggregation14,43, forming aggregates like those described here. As expected, however, the two distinct types of aggregates do not intermix (Supplementary Fig. 12A-D). Moreover, TCP are largely limited to pandemic lineages with two variants of its major pilin TcpA: Classical and El Tor44–46. In contrast to the results above, and as previously reported44, classical and El Tor strains formed uniformly mixed TCP-aggregates, indicating that the TcpA variants do not discriminate between one-another (Supplementary Fig. 12E).

The unusual tail of ATCC25872/V52 PilA is an inbuilt inhibitor of aggregation

To exclude the possibility that non-aggregating strains simply fail to make sufficient numbers of pili, *pilA*rep[Cys] variants of A1552-PilA (*pilA*rep[A1552; S67C]) and two non-aggregating alleles (*i.e. pilA*rep[Sa5Y; S67C]/[V52; N67C]) were constructed. These behaved similarly to the equivalent non-cysteine variant, though *pilA*rep[Sa5Y; S67C] has a modest transformation defect (Supplementary Fig. 13A-B). Both variants were piliated at similar levels to the A1552 control and in Δ*pilT* were hyper-piliated, although Sa5Y pili were generally very short (Fig. 5A-B). Hyper-piliation was especially clear for V52 pili, providing direct evidence that the inability of some alleles to aggregate is not due to a failure to produce sufficient numbers of pili but reflects a specific property of the pilin itself. Notably, detached pili of the *pilA*rep[A1552; S67C] variant assembled into large structures, as above, whereas those of the others did not (Supplementary Fig. 13C).

The V52/ATCC25872 PilA contains an unusual repetitive C-terminal extension (SGSGSGSGSGSGSGSGSGN), or ‘tail’. Here, we identified nine further examples of this tail, clustered into two well-separated phylogenetic groups (Supplementary Fig. 9). Moreover, 3/7 non-aggregating PilAs (*i.e. pilA*rep[V52]/[W6G]/[So5Y]) also contain a tail (Supplementary Fig. 9B). Removing the tail from V52-PilA *i.e. pilA*rep[V52Δtail], did not affect transformation (Fig. 5C). Remarkably, however, in cells lacking *pilT* it restored the ability to aggregate at levels indistinguishable from that of the A1552-PilA controls (Fig.

5D), and also demonstrated the ability to 'recognise' itself in co-culture experiments (Fig. 5E). These data suggest that the tail inhibits the ability of pili to aggregate, possibly by masking the site of pilus-pilus interaction. Indeed, a strain in which this tail was transplanted onto A1552-PilA (*i.e. pilA*rep[A1552+tail] remained highly transformable but was unable to aggregate (Fig. 5C-D). However, since efforts to label this PilA variant have so far been unsuccessful we cannot exclude another, non-specific effect.

DNA-uptake pili form networks on chitin surfaces

The data so far indicates that interactions between pili can mediate intercellular contacts. However, in liquid culture this requires artificial *tfoX* expression and the deletion of *pilT*. To investigate whether these interactions are relevant to the normal ecology of *V. cholerae* we visualised DNA-uptake pili produced by otherwise WT cells following cultivation on chitinous surfaces, upon which *tfoX* is naturally induced24,25. Strikingly, cells colonising the chitin surface produced large numbers of pili that frequently appeared to self-interact, forming dense networks of larger pili structures that overlie and interconnect the cells (Fig. 6A). Indeed, these structures were particularly evident at later time-points when extensive, mesh-like networks of pili extended across the entire chitin surface (Fig. 6B). Notably, although cells had now begun departing from the surface, these pili networks were retained within the detached pieces of biofilm (Fig. 6C). Control experiments confirmed that labelling on surfaces is specific and that these structures are DNA-uptake pili (Supplementary Fig. 14A). Moreover, although cells often appeared to posses multiple pili simultaneously (Supplementary Fig. 15A), upon the addition of exogenous DNA the majority of cells readily underwent DNA-uptake events, indicating that pilus retraction remains robust under these conditions (Supplementary Fig. 15B-C). Finally, using the *pilA*rep[Cys] variants described above, we directly compared the pili assembled on chitin surfaces by cells producing the aggregation-proficient A1552-PilA with those producing the aggregation-deficient V52-PilA. As expected, *pilA*rep[A1552; S67C] cells were also found within pili networks similar to those described above (Fig. 6D-E and Supplementary Fig. 16). In contrast, such networks were never observed for *pilA*rep[V52; N67C] cells. Surfaces were instead covered in what appeared to be mostly individual pili (Fig. 6 F-G and Fig S16).

An important caveat is that since the washing steps required for pilus staining tend to remove cells, but not pili, from the surface, the number of cells engaged in these networks is likely underestimated (Supplementary Fig. 14B). Given this observation, we hypothesised that DNA-uptake pili might bind to the chitin surface directly. Indeed, empty chitin beads incubated with either purified pili (Fig. 6H-I) or those naturally sheared off during liquid culture (Supplementary Fig. 17) rapidly became coated with pili. Moreover, attachment of A1552-PilA pili produced large self-interacting networks of pili (Fig. 6H and Supplementary Fig. 17). In contrast, pili composed of V52-PilA bound to the surface as individual filaments (Fig. 6I and Supplementary Fig. 17). Next, since DNA-uptake pili can bind directly to chitin surfaces we tested whether they play a role in chitin colonisation. However, in agreement with previous work24, Δ*pilA* cells had only a modest colonisation defect, especially compared to cells unable to assemble MSHA pili (Supplementary Fig. 18). In stark contrast, when we repeated these experiments under conditions of continuous mixing, to approximate the flow encountered in the natural environment, cells lacking *pilA* displayed a severe

colonisation defect comparable to that of Δ*mshA* and were outcompeted by the WT (Fig. 6J-L and Supplementary Fig. 19). Thus, these data support a model whereby DNA-uptake pili act downstream of MSHA pili, which are required for the initial attachment step16,24, acting to maintain or reinforce chitin colonisation. Indeed, all but one (TP-PilA) of the 16 *pilA* alleles studied here supported robust chitin colonisation under these conditions (Supplementary Fig. 20).

In summary, DNA-uptake pili bind chitin directly and are required for chitin colonisation under flow. Moreover, these data demonstrate that the aggregation phenotypes observed in liquid culture experiments report the natural ability of pili to self-interact and form networks on chitin surfaces. Finally, since the ability of DNA-uptake pili to bind chitin and their ability to self-interact appear to be distinct functions, the data suggests those capable of both likely have additional functions in chitin colonisation.

Discussion

Here we demonstrate that DNA-uptake pili are highly dynamic, that these dynamics are PilT-dependent, and that cells lacking *pilT* are minimally transformable, providing direct evidence for the longstanding model, whereby pilus retraction facilitates DNA-uptake. Indeed, our results on pilus dynamics are in close agreement with those recently reported by Ellison *et al.*, who notably, went on to demonstrate that the pilus binds directly to DNA47. The major finding of this work, however, is that DNA-uptake pili are able to interact and distinguish between one another in a sequence-specific manner. In liquid culture when retraction is deficient via the deletion of *pilT* this manifests as an exaggerated auto-aggregation phenotype, which we have used as a convenient tool to reveal and then investigate the ability of pili to self-interact. Since only a subpopulation of cells is piliated at any one time, and these pili are dynamic, eliminating retraction likely facilitates auto-aggregation by producing a homogenous population of hyper-piliated cells, thereby increasing the chances of interactions between pili. Work in *Neisseria meningitidis*, which auto-aggregates naturally at low levels but is dramatically enhanced by the deletion of *pilT*, supports this idea48. Importantly, however, the ability of pili to self-interact in artificial liquid culture conditions reflects a natural ability to interact on chitin surfaces. Indeed, under natural induction conditions on chitin surfaces, cells producing pili capable of aggregation elaborate multiple pili and form dense pili networks in an otherwise unmodified background, indicating that the chitin surface likely promotes interactions between pili. The proximity of cells to each other in the crowded surface environment might inherently foster these interactions. Alternatively, the altered physiology of cells growing on chitin might also impact pilus assembly via effects on the extension/retraction motors.

Our discovery that DNA-uptake pili bind chitin and are required for chitin colonisation under flow suggests an important role in the aquatic environment. Consequently, we propose that the primary function of DNA-uptake pili in the environment is likely not for natural transformation but rather for chitin colonisation. Indeed, as hypothesised elsewhere24,49, since pilus production is dependent on an intact chitin-utilisation pathway, colonisation mechanisms using DNA-uptake pili would be inherently selective for (i) nutritious chitinous surfaces and (ii) favour the recruitment and retention of productive cells while excluding

non-productive cells unable to make pili. In contrast, MSHA pili are produced constitutively and bind biotic and abiotic surfaces similarly16,19,20. Furthermore, the ability to interact not only with the surface but to mediate selective interactions with other cells would confer additional benefits that could act at multiple stages of colonisation. This might be particularly advantageous during early stages to bring smaller chitin particles together, and thus provide resistance to protozoan grazers, as well as at later stages to keep cells together during biofilm dispersal and thus, by allowing cells to arrive at a new niche in greater number, aid in persistence and dissemination. However, further work will be necessary to rule out the possibility that these interactions represent an ancient colonisation mechanism that has since been replaced. Nevertheless, the energetic cost of producing the pili networks we observe on chitin, the existence of a set of highly specific interactions, and the fact that in contrast to environmental isolates, pandemic strains all retain the same interaction-proficient PilA, argue for an on-going and important role.

Interestingly, auto-aggregation by TCP during virulence is essential for host colonisation13–15,43,44. Furthermore, TCP networks encasing cells on the intestinal cell surface have been suggested to protect cells from host defences50. Given the similarities between the two systems, especially our observation of dense pili networks on colonised chitin surfaces, we propose that the DNA-uptake pilus might play an analogous role in the aquatic environment. Indeed, ingestion of colonised chitin particles is thought to facilitate transmission to humans22,23 in cholera endemic areas and recovering cholera patients exhibit a strong immune response to PilA51. Thus, future work should investigate whether the networks of DNA-uptake pili we observed on chitin surfaces protect cells during this process.

In *N. gonorrhoeae*, artificially varying the density or post-translational modification state of pili leads to a form of cell-sorting based on differential interaction forces between pili52. This effect is likely related to aggregate dispersal during its infective lifestyle but does not permit specific recognition *per se*53. In contrast, the discovery here that natural PilA variability controls the ability of pili to self-interact, and creates highly specific interactions, provides a direct mechanism for kin recognition. The best-studied examples of kin recognition in microorganisms all involve adhesins and some form of aggregation (*e.g.* Flo1; *Saccharomyces cerevisiae*54, TgrB1-TgrC1; *Dictyostelium discoideum*55, and TraA; Myxobacteria56). In evolutionary terms, these recognition mechanisms are classified as ‘greenbeards’ because the cue, recognition of the cue and the resulting cooperative activity are all encoded by the same gene57,58. The ability of DNA-uptake pili to recognise and interact with pili composed of the same kind of PilA fits this classification and is therefore a specific form of greenbeard recognition57,58. However, this form of recognition implies close identity only at the greenbeard locus and so is better referred to as kind recognition57,58.

An important question going forward will be to understand what drives PilA diversity and how this is related to the type VI secretion system, which acts to kill non-kin bacteria59. Similarly, do those strains that lack the ability to self-interact employ alternative mechanisms (*e.g.* up-regulation of biofilm production) to colonise chitin surfaces? Indeed, the apparent acquisition of an inhibitor of pilus interactions by some PilA (*e.g.* ATCC25872/V52) hints that the ability to interact may not always be beneficial or else may reflect an

adaptation to a specific niche. Therefore, future work should focus on how the pili networks we observed on chitin surfaces contribute to the ecology of *V. cholerae*, especially under environmental conditions. Indeed, we still know relatively little about its natural lifestyle on chitin, partly due to the inherent technical difficulties associated with manipulating these surfaces. Nevertheless, the demonstration that in liquid media, specific interactions between pili composed of different major pilins is sufficient to enable segregation, provides a robust proof-of-concept that T4P have the capacity to function as a recognition mechanism. Finally, the fact that (i) T4P are widespread, (ii) auto-aggregation via T4P has been reported in multiple species60 and (iii) the major pilin subunit often varies3,39, raises the possibility that specific interactions between T4P could be relatively common and therefore represent an important contribution to bacterial kin recognition worthy of continued investigation.

Materials and Methods

Bacterial strains and plasmids

The bacterial strains used in this study are shown in Supplementary Table 1, together with the plasmids used and their construction. A1552, the *V. cholerae* strain used throughout this work61, is a fully-sequenced62 toxigenic O1 El Tor Inaba strain representative of the on-going 7th cholera pandemic, and was derived from a traveller entering the United States after being infected on a commercial aeroplane that took off in Peru63.

General methods

Bacterial cultures were grown aerobically at 30°C or 37°C, as required. Liquid medium used for growing bacterial strains was Lysogeny Broth (LB-Miller; 10 g/L NaCl, Carl Roth, Switzerland) and solid medium was LB agar. Where indicated, LB-S contained 20 g/L NaCl. Ampicillin (Amp; 100 μg/mL), gentamicin (Gent; 50 μg/mL), kanamycin (Kan; 75 μg/mL), streptomycin (Str; 100 μg/mL) and rifampicin (Rif; 100 μg/mL) were used for selection, as required. To induce expression from the P_{BAD} promoter, cultures were grown in media supplemented with 0.2% L-arabinose. Natural transformation of *V. cholerae* on chitin flakes was done in 0.5x DASW (defined artificial seawater), supplemented with vitamins (MEM, Gibco) and 50 mM HEPES, as previously described25. Counter-selection of phenylalanyl-tRNA synthetase (*pheS**) insertions (Trans2 method; see below) was done on medium supplemented with 20 mM 4-chloro-phenylalanine (cPhe; Sigma-Aldrich, Switzerland). Thiosulfate citrate bile salts sucrose (TCBS; Sigma-Aldrich, Switzerland) agar was used to counter-select for *E. coli* following bacterial mating. SacB-based counter-selection was done on NaCl-free medium containing 10 % sucrose.

Strain construction

DNA manipulations and *E. coli* transformations were carried out using standard methods64, and all constructs were verified by PCR and Sanger sequencing (Microsynth AG, Switzerland). Genetic engineering of *V. cholerae* was done using a combination of natural transformation and FLP-recombination; TransFLP65–67, *pheS**-based counter-selection; Trans268,69, and allelic exchange using bi-parental mating and the counter-selectable plasmid pGP704-Sac2824. The mini-Tn7 transposon carrying *araC* and various P_{BAD}-driven

genes was integrated into the large chromosome by tri-parental mating, as previously described70.

Chitin-independent competence induction

Chitin oligosaccharides resulting from growth on chitin trigger natural competence induction via the production of a master regulator, TfoX24,25,71–73. High cell-density, as sensed by quorum sensing via HapR, results in the production of an intermediate regulator QstR, which acts in concert with TfoX to regulate the transcription of a subset of the competence genes25,34,74,75. Therefore, to induce natural competence in liquid culture we used a well characterised and already validated chitin-independent approach that results in low levels of TfoX production34. This approach is based on the integration of a mini-Tn7 transposon into the large chromosome of *V. cholerae* containing an arabinose-inducible copy of *tfoX* (*i.e. araC*, P_{BAD}-*tfoX*), which we refer to as Tn*tfoX*. In the presence of inducer, strains carrying Tn*tfoX* turn on the expression of the competence genes according to the known regulatory pathways and upon reaching high cell-density are transformable at levels similar to those seen on chitin34. In the absence of inducer, competence genes are not produced and strains are non-transformable34.

Transformation frequency assay

Diverse strains harbouring Tn*tfoX* were tested for transformation using a chitin-independent transformation frequency assay, as previously described27,34. Briefly, overnight cultures were back-diluted 1:100 in fresh media with and without arabinose, as indicated, and grown 3h at 30°C with shaking (180 rpm). 0.5 mL aliquots of the cultures were mixed with 1 μg genomic DNA (derived from strain A1552-lacZ-Kan) in 1.5 mL eppendorf tubes and incubated 5h at 30°C with shaking (180 rpm), prior to serial dilution in PBS (phosphate buffered saline) and enumeration after overnight growth on LB media in the absence and presence of kanamycin. Transformation frequency was calculated as the number of transformants divided by the total number of bacteria.

Pilus shearing assay

Cultures were grown for 6h at 30°C with shaking (180 rpm) in 25 mL LB + 0.2% arabinose within a 125 mL Erlenmeyer flask. To shear pili from the cell surface, 10 mL culture was removed, vortexed at max speed for 1 min, and cells removed by three sequential centrifugation steps (10min; 4000 x *g*; 4°C). To the resulting supernatant saturated ammonium sulphate was added to 40% and incubated on ice for 1h. Precipitated proteins were recovered by centrifugation (30min; 20,000 x *g*; 4°C) and washed once with PBS. Samples were then re-suspended in 2x Laemmli buffer, boiled (15min; 95°C) and stored at -20°C until needed. To compare PilA levels between samples the re-suspension volume was normalised according to the optical density of the starting culture. Total protein controls were intact cell lysates. The relative amount of PilA in each sample was determined by Western blotting.

Aggregation assay

Overnight cultures were back-diluted 1:100 in the absence and presence of arabinose, as needed, and grown in 14 mL round bottom polystyrene test tubes (Falcon, Corning) on a carousel style rotary wheel (40 rpm) at 30°C. After 6h growth, aggregates were allowed to settle by standing the tube at RT for 30 min. The optical density at 600 nm ($O.D._{600}$) of the culture was then measured before and after mechanical disruption (vortex max speed; ~5 sec), which served to disperse any settled aggregates and return them to solution. Aggregation is expressed as the ratio of the $O.D._{600}$ Pre/Post-vortexing. For time-course experiments the standing time was reduced to 5 min. To visualise aggregates by microscopy overnight cultures were back-diluted either 1:100 individually or 1:200 when mixed, as needed, and were grown for 4h, as described above.

Microscopy

Cells were mounted on microscope slides coated with a thin agarose pad (1.2% w/v in PBS), covered with a #1 cover-slip, and were observed using a Zeiss Axio Imager M2 epi-fluorescence microscope attached to an AxioCam MRm camera and controlled by Zeiss AxioVision software. Image acquisition was done using a Plan-Apochromat 100×/1.4 Ph3 oil objective illuminated by an HXP120 lamp. Images were analysed and prepared for publication using ImageJ (http://rsb.info.nih.gov/ij).

Design and validation of PilA cysteine variants

To avoid the limitations imposed by immuno-fluorescent methods, we employed a cysteine labelling approach using a thiol-reactive dye33,76. PilA cysteine variants were created along the length of the surface exposed αβ-loop5,7 (Supplementary Fig. 1) and tested for functionality using a previously validated chitin-independent transformation system in which competence induction is arabinose-inducible34 (Tn*tfoX*; see above) (Fig. 1A, B and Supplementary Fig. 2A). A variant, PilA[S67C], was identified that is fully transformable (Fig. 1A), produced at similar levels (Supplementary Fig. 2B), and does not affect pilus assembly (Supplementary Fig. 2C), as assayed by a classical shearing method. Since other variants exhibited functional defects they were not studied further.

Pilus staining and quantification

Alexa Fluor™ 488 C_5 Maleimide (AF-488-Mal; Thermo Fisher Scientific; Cat# A10254) was dissolved in DMSO, aliquoted and stored at -20°C protected from light. Cultures used for staining were grown for 3.5h at 30°C on the rotary wheel, as above, in the absence and presence of competence induction, as required. To stain cells 100 μL of culture was mixed with dye at a final concentration of 25 μg/mL33 and incubated at RT for 5 min in the dark. Stained cells were harvested by centrifugation (5000 x *g*; 1 min), washed once with LB, re-suspended in 200 μL LB and imaged immediately. For quantification of piliation in snapshot imaging approximately 2000 cells per strain were analysed in each of three independent repeats. A subset of this data set was also analysed for the number of pili per cell and pilus length, as indicated in the text. For time-lapse analysis, images were acquired at RT at 10 sec intervals for 1 min (*i.e.* 7 frames). To analyse the number of pili produced per cell, per min,

5 fields of cells were analysed for each of the three independent repeats, yielding an analysis of 1947 cells in total.

Imaging on chitin surfaces

Visualisation of pilus production on chitin surfaces was done using chitin beads (NEB; Cat#S6651), which have previously been validated as a useful analogue for the natural chitin surface34,59. Prior to use, chitin beads were washed 5x with 0.5x DASW + 50 mM HEPES + vitamins. Colonisation of chitin beads was done in 12-well culture plates (Cellstar) by mixing 0.1 mL washed O/N culture with 0.1 mL washed beads in a final volume of 1 mL 0.5x DASW + 50 mM HEPES + vitamins, and incubated at 30°C for 48h. Pilus staining was done as described above except that the final re-suspension volume was reduced to 50 μL. Stained beads were mounted directly on glass microscope slides, covered with a #1 cover-slip and imaged using either a Plan-Apochromat 100x/1.4 Ph3 or Plan-Neofluar 40x/1.3 Ph3 oil objective, as needed. To image cells after prolonged incubation (≥72h), plates were incubated within a homemade humidified chamber. Chitin colonisation under conditions of continuous mixing was done in 14 mL bottom polystyrene test tubes (Falcon, Corning) by mixing 0.2 mL washed O/N culture with 0.2 mL washed beads in a final volume of 2 mL, and incubated at 30°C for 48h on a carousel style rotary wheel (40 rpm). To avoid damaging the beads manipulations were done using wide bore tips.

Chitin binding activity of DNA-uptake pili

Cultures of strains encoding PilA cysteine variants were grown under chitin-independent competence induction for 5h at 30°C on a rotary wheel, as described above. To shear pili from the cell surface, 0.5 mL culture was removed, vortexed at max speed for 1 min, and cells removed by centrifugation (5min; 5000 x *g*). Next, either 0.1 mL of sheared pili or 0.1 mL of untreated cell culture, as indicated in the text, were mixed with 0.1 mL washed chitin beads in 0.5x DASW + 50 mM HEPES + vitamins and incubated flat in a 1.5 mL eppendorf tube with shaking (30°C; 180rpm; 1h). Bound pili were then stained with AF-488-Mal, as described above, washed once with 0.8 mL LB and re-suspended in a final volume of 0.1 mL LB.

Western blotting

Cell lysates were prepared by suspending harvested cells in 2x Laemmli buffer (100 μL buffer per O.D. unit) before boiling at 95°C for 15 min. Proteins were separated by SDS-PAGE using a 15% resolving gel and blotted onto PVDF membranes using a wet-transfer apparatus. Immuno-detection was performed as described previously34. Primary anti-PilA antibodies were raised in rabbits against synthetic peptides of A1552 PilA (Eurogentec, Belgium; #1510525) and used at a dilution of 1:5000. Anti-Rabbit IgG HRP (Sigma; Cat# A9169) diluted 1:5000 was used as a secondary antibody. Sample loading was verified with Direct-Blot™ HRP anti-*E. coli* RNA Sigma70 (BioLegend; Cat# 663205) diluted 1:10,000.

Motility assay

To quantity motility phenotypes 2 μL overnight culture was spotted onto soft LB agar (0.3%) plates (two technical replicates) and incubated at RT for 24h prior to photography. The

swarming diameter (cm) was measured and is expressed as the mean of three independent biological repeats. A flagellin-deficient (Δ*flaA*) non-motile strain was used as a negative control.

Bioinformatics of PilA diversity

Vibrio cholerae genomes were obtained from NCBI (National Center for Biotechnology Information), and are listed in Supplementary File 1. Geneious software (10.2.3)77 was used to perform custom BLAST analyses and identify *pilA*. Unique PilA sequences were extracted and combined with the PilA sequences from strain A1552 and a collection of environmental isolates78,79, as deduced by Sanger sequencing (Supplementary File 2), as indicated in the text. PilA sequences were aligned with Muscle and a consensus neighbour-joining tree constructed using the Jukes-Cantor substitution model, resampled with 100 bootstrap replicates. MshA from strain A1552 was used as an outgroup.

Statistics and Reproducibility

All data are representative of the results of three independent biological repeats. All experiments were repeated independently three times, with similar results. Bar graphs display the mean value, error bars display the standard deviation, and are overlaid by dot plots to indicate the distribution of the individual data points.

Supplementary Material

Refer to Web version on PubMed Central for supplementary material.

Acknowledgements

We thank members of the Blokesch lab for scientific discussions and Ivan Mateus-Gonzalez for assistance with bioinformatics analyses. We further thank A. Boehm, S. Pukatzki, J. Mekalanos, J. Reidl, and members of the Institut National de Recherche Biomédicale of the Democratic Republic of the Congo, for providing *V. cholerae* strains and V. Pelicic for advice on *pheS*-mediated counter-selection. Work on this problem was supported by a Marie Skłodowska-Curie Individual Fellowship (703340; CMDNAUP) to D.W.A. and by EPFL intramural funding and an ERC Starting (309064-VIR4ENV) and Consolidator (724630-CholeraIndex) Grant from the European Research Council to MB. M.B. is a Howard Hughes Medical Institute (HHMI) International Research Scholar (Grant# 55008726).

References

1. Maier B, Wong GCL. How Bacteria Use Type IV Pili Machinery on Surfaces. Trends in microbiology. 2015; 23:775–788. DOI: 10.1016/j.tim.2015.09.002 [PubMed: 26497940]
2. Berry JL, Pelicic V. Exceptionally widespread nanomachines composed of type IV pilins: the prokaryotic Swiss Army knives. FEMS microbiology reviews. 2015; 39:134–154. DOI: 10.1093/femsre/fuu001 [PubMed: 25793961]
3. Giltner CL, Nguyen Y, Burrows LL. Type IV pilin proteins: versatile molecular modules. Microbiology and molecular biology reviews : MMBR. 2012; 76:740–772. DOI: 10.1128/MMBR.00035-12 [PubMed: 23204365]
4. Chang YW, et al. Architecture of the type IVa pilus machine. Science. 2016; 351:aad2001.doi: 10.1126/science.aad2001 [PubMed: 26965631]
5. Craig L, et al. Type IV pilus structure by cryo-electron microscopy and crystallography: implications for pilus assembly and functions. Molecular cell. 2006; 23:651–662. DOI: 10.1016/j.molcel.2006.07.004 [PubMed: 16949362]

6. Gold VA, Salzer R, Averhoff B, Kuhlbrandt W. Structure of a type IV pilus machinery in the open and closed state. eLife. 2015; 4doi: 10.7554/eLife.07380
7. Kolappan S, et al. Structure of the *Neisseria meningitidis* Type IV pilus. Nature communications. 2016; 7doi: 10.1038/ncomms13015
8. Merz AJ, So M, Sheetz MP. Pilus retraction powers bacterial twitching motility. Nature. 2000; 407:98–102. DOI: 10.1038/35024105 [PubMed: 10993081]
9. Skerker JM, Berg HC. Direct observation of extension and retraction of type IV pili. Proceedings of the National Academy of Sciences of the United States of America. 2001; 98:6901–6904. DOI: 10.1073/pnas.121171698 [PubMed: 11381130]
10. Jakovljevic V, Leonardy S, Hoppert M, Sogaard-Andersen L. PilB and PilT are ATPases acting antagonistically in type IV pilus function in *Myxococcus xanthus*. Journal of bacteriology. 2008; 190:2411–2421. DOI: 10.1128/JB.01793-07 [PubMed: 18223089]
11. McCallum M, Tammam S, Khan A, Burrows LL, Howell PL. The molecular mechanism of the type IVa pilus motors. Nature communications. 2017; 8doi: 10.1038/ncomms15091
12. Waldor MK, Mekalanos JJ. Lysogenic conversion by a filamentous phage encoding cholera toxin. Science. 1996; 272:1910–1914. [PubMed: 8658163]
13. Chiang SL, Taylor RK, Koomey M, Mekalanos JJ. Single amino acid substitutions in the N-terminus of *Vibrio cholerae* TcpA affect colonization, autoagglutination, and serum resistance. Molecular microbiology. 1995; 17:1133–1142. [PubMed: 8594332]
14. Taylor RK, Miller VL, Furlong DB, Mekalanos JJ. Use of *phoA* gene fusions to identify a pilus colonization factor coordinately regulated with cholera toxin. Proceedings of the National Academy of Sciences of the United States of America. 1987; 84:2833–2837. [PubMed: 2883655]
15. Kirn TJ, Lafferty MJ, Sandoe CM, Taylor RK. Delineation of pilin domains required for bacterial association into microcolonies and intestinal colonization by *Vibrio cholerae*. Molecular microbiology. 2000; 35:896–910. [PubMed: 10692166]
16. Chiavelli DA, Marsh JW, Taylor RK. The mannose-sensitive hemagglutinin of *Vibrio cholerae* promotes adherence to zooplankton. Applied and environmental microbiology. 2001; 67:3220–3225. DOI: 10.1128/AEM.67.7.3220-3225.2001 [PubMed: 11425745]
17. Moorthy S, Watnick PI. Genetic evidence that the *Vibrio cholerae* monolayer is a distinct stage in biofilm development. Molecular microbiology. 2004; 52:573–587. DOI: 10.1111/j.1365-2958.2004.04000.x [PubMed: 15066042]
18. Utada AS, et al. *Vibrio cholerae* use pili and flagella synergistically to effect motility switching and conditional surface attachment. Nature communications. 2014; 5:4913.doi: 10.1038/ncomms5913
19. Watnick PI, Fullner KJ, Kolter R. A role for the mannose-sensitive hemagglutinin in biofilm formation by *Vibrio cholerae* El Tor. Journal of bacteriology. 1999; 181:3606–3609. [PubMed: 10348878]
20. Watnick PI, Kolter R. Steps in the development of a *Vibrio cholerae* El Tor biofilm. Molecular microbiology. 1999; 34:586–595. [PubMed: 10564499]
21. Tamplin ML, Gauzens AL, Huq A, Sack DA, Colwell RR. Attachment of *Vibrio cholerae* serogroup O1 to zooplankton and phytoplankton of Bangladesh waters. Applied and environmental microbiology. 1990; 56:1977–1980. [PubMed: 2383016]
22. Blokesch M. Competence-induced type VI secretion might foster intestinal colonization by *Vibrio cholerae*: Intestinal interbacterial killing by competence-induced *V. cholerae*. BioEssays : news and reviews in molecular, cellular and developmental biology. 2015; 37:1163–1168. DOI: 10.1002/bies.201500101
23. Colwell RR, et al. Reduction of cholera in Bangladeshi villages by simple filtration. Proceedings of the National Academy of Sciences of the United States of America. 2003; 100:1051–1055. DOI: 10.1073/pnas.0237386100 [PubMed: 12529505]
24. Meibom KL, et al. The *Vibrio cholerae* chitin utilization program. Proceedings of the National Academy of Sciences of the United States of America. 2004; 101:2524–2529. [PubMed: 14983042]
25. Meibom KL, Blokesch M, Dolganov NA, Wu CY, Schoolnik GK. Chitin induces natural competence in *Vibrio cholerae*. Science. 2005; 310:1824–1827. DOI: 10.1126/science.1120096 [PubMed: 16357262]

26. Johnston C, Martin B, Fichant G, Polard P, Claverys JP. Bacterial transformation: distribution, shared mechanisms and divergent control. Nature reviews. Microbiology. 2014; 12:181–196. DOI: 10.1038/nrmicro3199 [PubMed: 24509783]
27. Seitz P, Blokesch M. DNA-uptake machinery of naturally competent *Vibrio cholerae*. Proceedings of the National Academy of Sciences of the United States of America. 2013; 110:17987–17992. DOI: 10.1073/pnas.1315647110 [PubMed: 24127573]
28. Seitz P, et al. ComEA is essential for the transfer of external DNA into the periplasm in naturally transformable *Vibrio cholerae* cells. PLoS genetics. 2014; 10:e1004066.doi: 10.1371/journal.pgen.1004066 [PubMed: 24391524]
29. Seitz P, Blokesch M. DNA transport across the outer and inner membranes of naturally transformable *Vibrio cholerae* is spatially but not temporally coupled. mBio. 2014; 5doi: 10.1128/mBio.01409-14
30. Wolfgang M, et al. PilT mutations lead to simultaneous defects in competence for natural transformation and twitching motility in piliated *Neisseria gonorrhoeae*. Molecular microbiology. 1998; 29:321–330. [PubMed: 9701824]
31. Gangel H, et al. Concerted spatio-temporal dynamics of imported DNA and ComE DNA uptake protein during gonococcal transformation. PLoS pathogens. 2014; 10:e1004043.doi: 10.1371/journal.ppat.1004043 [PubMed: 24763594]
32. Laurenceau R, et al. A type IV pilus mediates DNA binding during natural transformation in *Streptococcus pneumoniae*. PLoS pathogens. 2013; 9:e1003473.doi: 10.1371/journal.ppat.1003473 [PubMed: 23825953]
33. Ellison CK, et al. Obstruction of pilus retraction stimulates bacterial surface sensing. Science. 2017; 358:535–538. DOI: 10.1126/science.aan5706 [PubMed: 29074778]
34. Lo Scrudato M, Blokesch M. The regulatory network of natural competence and transformation of *Vibrio cholerae*. PLoS genetics. 2012; 8:e1002778.doi: 10.1371/journal.pgen.1002778 [PubMed: 22737089]
35. Jones CJ, et al. C-di-GMP Regulates Motile to Sessile Transition by Modulating MshA Pili Biogenesis and Near-Surface Motility Behavior in *Vibrio cholerae*. PLoS pathogens. 2015; 11:e1005068.doi: 10.1371/journal.ppat.1005068 [PubMed: 26505896]
36. Fong JC, Syed KA, Klose KE, Yildiz FH. Role of Vibrio polysaccharide (vps) genes in VPS production, biofilm formation and *Vibrio cholerae* pathogenesis. Microbiology. 2010; 156:2757–2769. DOI: 10.1099/mic.0.040196-0 [PubMed: 20466768]
37. Biais N, Ladoux B, Higashi D, So M, Sheetz M. Cooperative retraction of bundled type IV pili enables nanonewton force generation. PLoS biology. 2008; 6:e87.doi: 10.1371/journal.pbio.0060087 [PubMed: 18416602]
38. Joelsson A, Liu Z, Zhu J. Genetic and phenotypic diversity of quorum-sensing systems in clinical and environmental isolates of *Vibrio cholerae*. Infection and immunity. 2006; 74:1141–1147. DOI: 10.1128/IAI.74.2.1141-1147.2006 [PubMed: 16428762]
39. Aagesen AM, Häse CC. Sequence analyses of type IV pili from *Vibrio cholerae, Vibrio parahaemolyticus*, and *Vibrio vulnificus*. Microbial ecology. 2012; 64:509–524. DOI: 10.1007/s00248-012-0021-2 [PubMed: 22383120]
40. Aldova E, Laznickova K, Stepankova E, Lietava J. Isolation of nonagglutinable vibrios from an enteritis outbreak in Czechoslovakia. The Journal of infectious diseases. 1968; 118:25–31. [PubMed: 5640984]
41. Chun J, et al. Comparative genomics reveals mechanism for short-term and long-term clonal transitions in pandemic *Vibrio cholerae*. Proceedings of the National Academy of Sciences of the United States of America. 2009; 106:15442–15447. DOI: 10.1073/pnas.0907787106 [PubMed: 19720995]
42. Li M, Shimada T, Morris JG Jr, Sulakvelidze A, Sozhamannan S. Evidence for the emergence of non-O1 and non-O139 *Vibrio cholerae* strains with pathogenic potential by exchange of O-antigen biosynthesis regions. Infection and immunity. 2002; 70:2441–2453. [PubMed: 11953381]
43. DiRita VJ, Neely M, Taylor RK, Bruss PM. Differential expression of the ToxR regulon in classical and E1 Tor biotypes of *Vibrio cholerae* is due to biotype-specific control over toxT

expression. Proceedings of the National Academy of Sciences of the United States of America. 1996; 93:7991–7995. [PubMed: 8755590]

44. Jude BA, Taylor RK. The physical basis of type 4 pilus-mediated microcolony formation by *Vibrio cholerae* O1. Journal of structural biology. 2011; 175:1–9. DOI: 10.1016/j.jsb.2011.04.008 [PubMed: 21527347]
45. Lim MS, et al. *Vibrio cholerae* El Tor TcpA crystal structure and mechanism for pilus-mediated microcolony formation. Molecular microbiology. 2010; 77:755–770. DOI: 10.1111/j.1365-2958.2010.07244.x [PubMed: 20545841]
46. Rhine JA, Taylor RK. TcpA pilin sequences and colonization requirements for O1 and O139 *Vibrio cholerae*. Molecular microbiology. 1994; 13:1013–1020. [PubMed: 7854116]
47. Ellison CK, et al. Retraction of DNA-bound type IV competence pili initiates DNA uptake during natural transformation in *Vibrio cholerae*. Nature microbiology. 2018; 3:773–780. DOI: 10.1038/s41564-018-0174-y
48. Hélaine S, et al. PilX, a pilus-associated protein essential for bacterial aggregation, is a key to pilus-facilitated attachment of *Neisseria meningitidis* to human cells. Molecular microbiology. 2005; 55:65–77. DOI: 10.1111/j.1365-2958.2004.04372.x [PubMed: 15612917]
49. Shime-Hattori A, et al. Two type IV pili of *Vibrio parahaemolyticus* play different roles in biofilm formation. FEMS microbiology letters. 2006; 264:89–97. DOI: 10.1111/j.1574-6968.2006.00438.x [PubMed: 17020553]
50. Krebs SJ, Taylor RK. Protection and attachment of *Vibrio cholerae* mediated by the toxin-coregulated pilus in the infant mouse model. Journal of bacteriology. 2011; 193:5260–5270. DOI: 10.1128/JB.00378-11 [PubMed: 21804008]
51. Hang L, et al. Use of in vivo-induced antigen technology (IVIAT) to identify genes uniquely expressed during human infection with *Vibrio cholerae*. Proceedings of the National Academy of Sciences of the United States of America. 2003; 100:8508–8513. DOI: 10.1073/pnas.1431769100 [PubMed: 12826608]
52. Oldewurtel ER, Kouzel N, Dewenter L, Henseler K, Maier B. Differential interaction forces govern bacterial sorting in early biofilms. eLife. 2015; 4doi: 10.7554/eLife.10811
53. Chamot-Rooke J, et al. Posttranslational modification of pili upon cell contact triggers *N. meningitidis* dissemination. Science. 2011; 331:778–782. DOI: 10.1126/science.1200729 [PubMed: 21311024]
54. Smukalla S, et al. FLO1 is a variable green beard gene that drives biofilm-like cooperation in budding yeast. Cell. 2008; 135:726–737. DOI: 10.1016/j.cell.2008.09.037 [PubMed: 19013280]
55. Hirose S, Benabentos R, Ho HI, Kuspa A, Shaulsky G. Self-recognition in social amoebae is mediated by allelic pairs of tiger genes. Science. 2011; 333:467–470. DOI: 10.1126/science.1203903 [PubMed: 21700835]
56. Pathak DT, Wei X, Dey A, Wall D. Molecular recognition by a polymorphic cell surface receptor governs cooperative behaviors in bacteria. PLoS genetics. 2013; 9:e1003891.doi: 10.1371/journal.pgen.1003891 [PubMed: 24244178]
57. Strassmann JE, Gilbert OM, Queller DC. Kin discrimination and cooperation in microbes. Annual review of microbiology. 2011; 65:349–367. DOI: 10.1146/annurev.micro.112408.134109
58. Wall D. Kin Recognition in Bacteria. Annual review of microbiology. 2016; 70:143–160. DOI: 10.1146/annurev-micro-102215-095325
59. Borgeaud S, Metzger LC, Scrignari T, Blokesch M. The type VI secretion system of *Vibrio cholerae* fosters horizontal gene transfer. Science. 2015; 347:63–67. DOI: 10.1126/science.1260064 [PubMed: 25554784]
60. Trunk T, Khalil HS, Leo JC. Bacterial autoaggregation. AIMS Microbiology. 2018; 4:140–164. DOI: 10.3934/microbiol.2018.1.140 [PubMed: 31294207]
61. Yildiz FH, Schoolnik GK. Role of *rpoS* in stress survival and virulence of *Vibrio cholerae*. Journal of bacteriology. 1998; 180:773–784. [PubMed: 9473029]
62. Matthey N, Drebes Dörr NC, Blokesch M. Long-Read-Based Genome Sequences of Pandemic and Environmental *Vibrio cholerae* Strains. Microbiology resource announcements. 2018; 7doi: 10.1128/MRA.01574-18

63. Blokesch M. A quorum sensing-mediated switch contributes to natural transformation of *Vibrio cholerae*. Mobile genetic elements. 2012; 2:224–227. DOI: 10.4161/mge.22284 [PubMed: 23446800]
64. Sambrook, J, Fritsch, EF, Maniatis, T. Molecular Cloning: A Laboratory Manual. Cold Spring Harbor: Cold Spring Harbor Laboratory Press; 1989.
65. De Souza Silva O, Blokesch M. Genetic manipulation of *Vibrio cholerae* by combining natural transformation with FLP recombination. Plasmid. 2010; 64:186–195. DOI: 10.1016/j.plasmid.2010.08.001 [PubMed: 20709100]
66. Marvig RL, Blokesch M. Natural transformation of *Vibrio cholerae* as a tool - optimizing the procedure. BMC microbiology. 2010; 10:155.doi: 10.1186/1471-2180-10-155 [PubMed: 20509862]
67. Blokesch M. TransFLP--a method to genetically modify *Vibrio cholerae* based on natural transformation and FLP-recombination. Journal of visualized experiments : JoVE. 2012; 68:e3761.doi: 10.3791/3761
68. Van der Henst C, et al. Molecular insights into *Vibrio cholerae*'s intra-amoebal host-pathogen interactions. Nature communications. 2018; 9doi: 10.1038/s41467-018-05976-x
69. Gurung I, Berry JL, Hall AMJ, Pelicic V. Cloning-independent markerless gene editing in *Streptococcus sanguinis*: novel insights in type IV pilus biology. Nucleic acids research. 2017; 45:e40.doi: 10.1093/nar/gkw1177 [PubMed: 27903891]
70. Bao Y, Lies DP, Fu H, Roberts GP. An improved Tn7-based system for the single-copy insertion of cloned genes into chromosomes of gram-negative bacteria. Gene. 1991; 109:167–168. [PubMed: 1661697]
71. Yamamoto S, et al. Regulation of natural competence by the orphan two-component system sensor kinase ChiS involves a non-canonical transmembrane regulator in *Vibrio cholerae*. Molecular microbiology. 2014; 91:326–347. DOI: 10.1111/mmi.12462 [PubMed: 24236404]
72. Dalia AB, Lazinski DW, Camilli A. Identification of a membrane-bound transcriptional regulator that links chitin and natural competence in *Vibrio cholerae*. mBio. 2014; 5:e01028–01013. DOI: 10.1128/mBio.01028-13 [PubMed: 24473132]
73. Yamamoto S, et al. Identification of a chitin-induced small RNA that regulates translation of the tfoX gene, encoding a positive regulator of natural competence in Vibrio cholerae. Journal of bacteriology. 2011; 193:1953–1965. DOI: 10.1128/JB.01340-10 [PubMed: 21317321]
74. Lo Scrudato M, Blokesch M. A transcriptional regulator linking quorum sensing and chitin induction to render *Vibrio cholerae* naturally transformable. Nucleic acids research. 2013; 41:3644–3658. DOI: 10.1093/nar/gkt041 [PubMed: 23382174]
75. Jaskólska M, Stutzmann S, Stoudmann C, Blokesch M. QstR-dependent regulation of natural competence and type VI secretion in *Vibrio cholerae*. Nucleic acids research. 2018; 46:10619–10634. DOI: 10.1093/nar/gky717 [PubMed: 30102403]
76. Blair KM, Turner L, Winkelman JT, Berg HC, Kearns DB. A molecular clutch disables flagella in the *Bacillus subtilis* biofilm. Science. 2008; 320:1636–1638. DOI: 10.1126/science.1157877 [PubMed: 18566286]
77. Kearse M, et al. Geneious Basic: an integrated and extendable desktop software platform for the organization and analysis of sequence data. Bioinformatics. 2012; 28:1647–1649. DOI: 10.1093/bioinformatics/bts199 [PubMed: 22543367]
78. Keymer DP, Miller MC, Schoolnik GK, Boehm AB. Genomic and phenotypic diversity of coastal *Vibrio cholerae* strains is linked to environmental factors. Applied and environmental microbiology. 2007; 73:3705–3714. DOI: 10.1128/AEM.02736-06 [PubMed: 17449702]
79. Purdy A, Rohwer F, Edwards R, Azam F, Bartlett DH. A glimpse into the expanded genome content of *Vibrio cholerae* through identification of genes present in environmental strains. Journal of bacteriology. 2005; 187:2992–3001. DOI: 10.1128/JB.187.9.2992-3001.2005 [PubMed: 15838025]

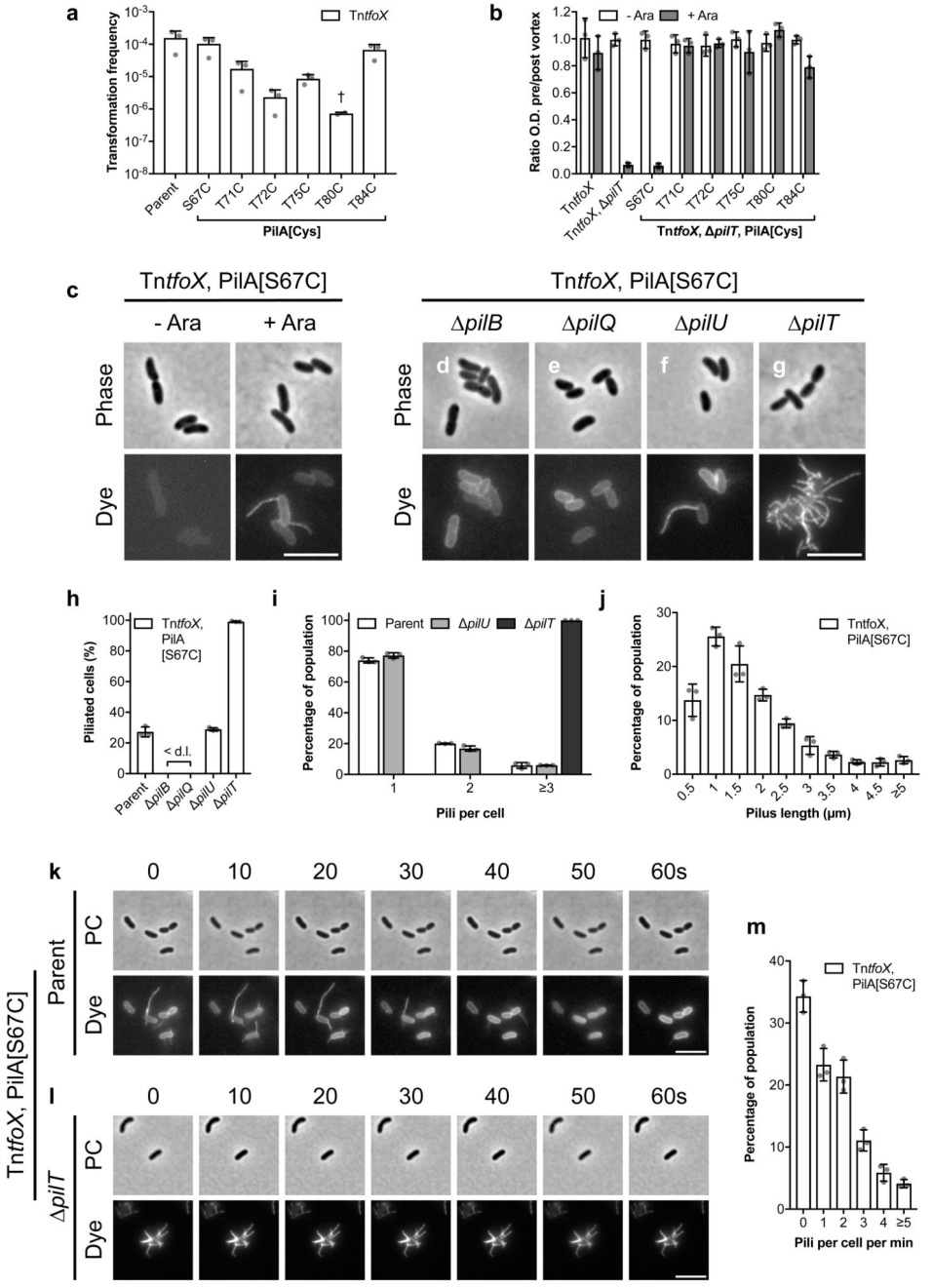

Figure 1. Direct observation of dynamic DNA-uptake pili.

(**A**) Functionality of PilA cysteine variants (PilA[Cys]) in a chitin-independent transformation assay using strains carrying an arabinose-inducible copy of *tfoX* (Tn*tfoX*). Transformation frequencies are the mean of three independent biological repeats (+S.D.). < d.l., below detection limit. †, < d.l. in one repeat.

(**B**) Effect of PilA cysteine variants on the ability of retraction deficient (Tn*tfoX*, Δ*pilT*) cells to aggregate. Aggregation is shown as the ratio of the culture optical density ($O.D._{600}$)

Europe PMC Funders Author Manuscripts

before and after vortexing, in the absence (- Ara) and presence (+ Ara) of *tfoX* induction, as indicated. Values are the mean of three independent biological repeats (±S.D.).

(**C**-**G**) Snapshot imaging of pili in cells of A1552-Tn*tfoX*, PilA[S67C] and its derivatives. (**C**) Cells of A1552-Tn*tfoX*, PilA[S67C] were grown in the absence (- Ara) and presence (+ Ara) of *tfoX* induction, as indicated, and stained with AF-488-Mal. Bar = 5 μm. (D-E) Cells of A1552-Tn*tfoX*, PilA[S67C] were grown in the presence of *tfoX* induction and stained with AF-488-Mal in a (**D**) Δ*pilB*, (**E**) Δ*pilQ*, (**F**) Δ*pilU* and (**G**) Δ*pilT* background, as indicated. Bar = 5 μm.

(**H**-**J**) Quantification of piliation in snapshot imaging. Bars represent the mean of three repeats (±S.D.). (**H**) Percentage of piliated cells in the indicated backgrounds. *n* = *c.a.* 2000 cells per strain per repeat. (**I**) Histogram of number of pili per cell in piliated cells in WT parent (A1552-Tn*tfoX*, PilA[S67C]), Δ*pilU* (A1552-Tn*tfoX*, PilA[S67C], Δ*pilU*) and Δ*pilT* (A1552-Tn*tfoX*, PilA[S67C], Δ*pilT*) backgrounds, as indicated. *n* = *c.a.* 300 cells per strain per repeat. (**J**) Histogram of pilus length in cells of A1552-Tn*tfoX*, PilA[S67C]. *n* = *c.a.* 500-600 cells per repeat.

(**K**-**L**) Time-lapse series of pilus dynamics in (**K**) WT parent (A1552-Tn*tfoX*, PilA[S67C]) and (**L**) Δ*pilT* (A1552-Tn*tfoX*, PilA[S67C], Δ*pilT*) backgrounds. Cells were stained with AF-488-Mal and imaged at 10s intervals for 1 minute. Upper panels show phase-contrast (PC), lower panels show fluorescence (dye). Time in seconds (s), as indicated. Bars = 5 μm.

(**M**) Histogram showing quantification of pili produced per cell per min in the WT parent (A1552-Tn*tfoX*, PilA[S67C]) background. Bars represent the mean of three repeats (±S.D.). *n* = *c.a.* 500-700 cells per repeat.

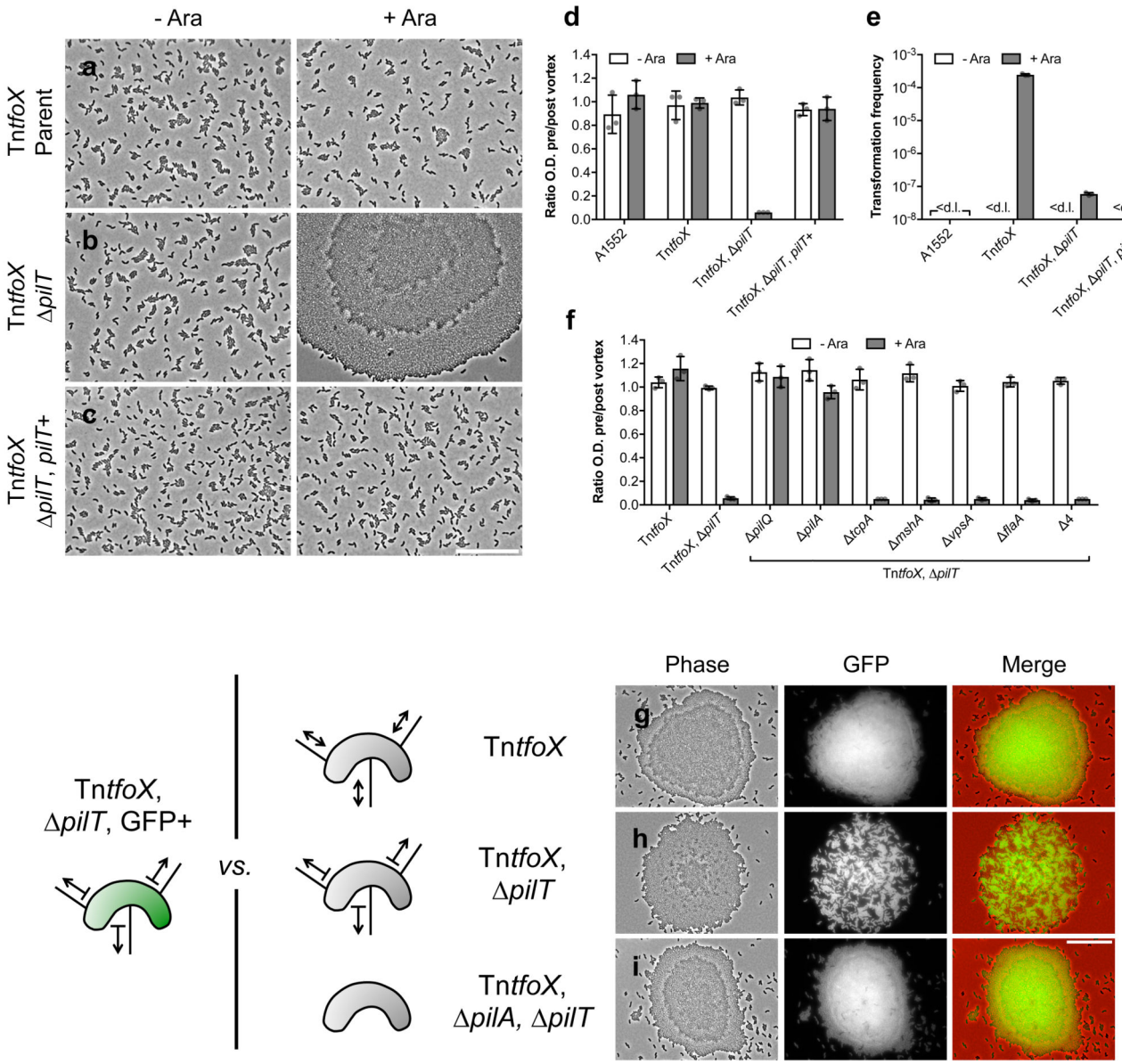

Figure 2. Competent cells auto-aggregate in the absence of pilus retraction.

(**A**-**C**) Phase-contrast microscopy of cells of strains (**A**) A1552-Tn*tfoX*, (**B**) A1552-Tn*tfoX*, Δ*pilT* and (**C**) A1552-Tn*tfoX*, Δ*pilT*, *pilT*+, grown in the absence (- Ara) and presence (+ Ara) of *tfoX* induction, as indicated. PilT complementation (*pilT+*) was achieved by placing an intact copy of *pilT* driven by its native promoter at a neutral ectopic locus. Scale bar = 25 μm.

(**D**-**E**) Aggregation and transformation frequency of cells of strains A1552-Tn*tfoX*, A1552-Tn*tfoX*, Δ*pilT* and A1552-Tn*tfoX*, Δ*pilT*, *pilT*+, grown in the absence (- Ara) and presence (+ Ara) of *tfoX* induction, as indicated. A1552 (without inducible *tfoX*) was used as a negative control. (**D**) Aggregation is shown as the ratio of the culture optical density (O.D. $_{600}$) before and after vortexing. Values are the mean of three repeats (±S.D.). (**E**) Chitin-

Europe PMC Funders Author Manuscripts

independent transformation frequency assay. Values are the mean of three repeats (+S.D.). < d.l., below detection limit.

(**F**) Effect of various deletion backgrounds on the ability of retraction deficient cells to aggregate. Aggregation is shown as the ratio of the culture optical density ($O.D._{600}$) before and after vortexing, in the absence (- Ara) and presence (+ Ara) of *tfoX* induction, as indicated. Δ4 = Δ*tcpA*, Δ*mshA*, Δ*vpsA*, Δ*flaA* quadruple mutant. Values are the mean of three repeats (±S.D.).

(**G-I**) Co-culture of fluorescent Δ*pilT* cells (A1552-Tn*tfoX*, Δ*pilT*, GFP+) producing GFP and non-fluorescent cells of the (**G**) WT parent (A1552-Tn*tfoX*), (**H**) Δ*pilT* (A1552-Tn*tfoX*, Δ*pilT*) and (**I**) Δ*pilA*, Δ*pilT* (A1552-Tn*tfoX*, Δ*pilA*, Δ*pilT*), grown in the presence of *tfoX* induction. Merged images show GFP in green and phase-contrast in red. Bar = 25 μm.

Europe PMC Funders Author Manuscripts

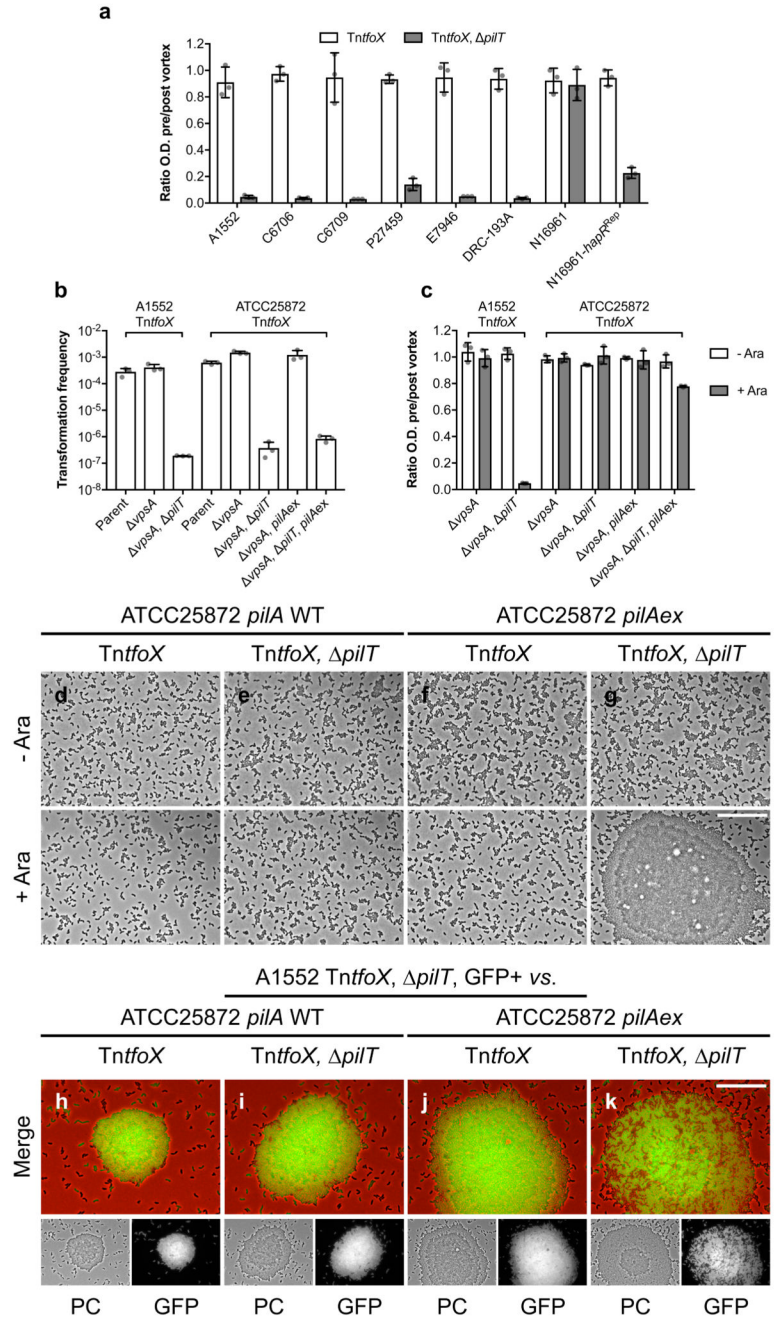

Figure 3. A1552 PilA is sufficient for aggregation in a non-pandemic strain.

(**A**) Aggregation of representative 7th pandemic strains of *V. cholerae*, including the effect of *hapR*^{Rep} on N16961, in a Tn*tfoX* and a Tn*tfoX*, Δ*pilT* background, as indicated. Aggregation is shown as the ratio of the culture optical density (O.D. $_{600}$) before and after vortexing, in the presence of *tfoX* induction. Values are the mean of three repeats (±S.D.). (**B**-**C**) Transformation frequency and aggregation of *V. cholerae* strain ATCC25872-Tn*tfoX* compared to that of A1552-Tn*tfoX*. (**B**) Chitin-independent transformation assay. Transformation frequencies are the mean of three repeats (+S.D.). (**C**) Aggregation is shown

as the ratio of the culture optical density (O.D. $_{600}$) before and after vortexing, in the absence (- Ara) and presence (+ Ara) of *tfoX* induction, as indicated. Values are the mean of three repeats (±S.D.).

(**D**-**G**) Phase-contrast microscopy of ATCC25872-Tn*tfoX*, Δ*vpsA* cells carrying (**D** and **E**) their native *pilA* (*pilA* WT) and (**F** and **G**) A1552 *pilA* (*pilA*ex), in a (**D** and **F**) *pilT*+ and (**E** and **G**) Δ*pilT* background, as indicated. Strains were cultured in the absence (- Ara) and presence (+ Ara), as indicated. Bar = 25 μm. Note that ATCC25872 derivatives were co-deleted for *vpsA* to rule out any compounding effects of biofilm formation.

(**H**-**K**) Co-culture of fluorescent cells of A1552-Tn*tfoX*, Δ*pilT*, GFP+, producing GFP, and non-fluorescent cells of ATCC25872-Tn*tfoX*, Δ*vpsA* carrying (**H** and **I**) their native *pilA* (*pilA* WT) and (**J** and **K**) A1552 PilA (*pilA*ex), in a (**H** and **J**) *pilT*+ and (**I** and **K**) Δ*pilT* background, as indicated. Cells were grown in the presence of *tfoX* induction. Merged images show GFP in green and phase-contrast (PC) in red. Bar = 25 μm.

Europe PMC Funders Author Manuscripts

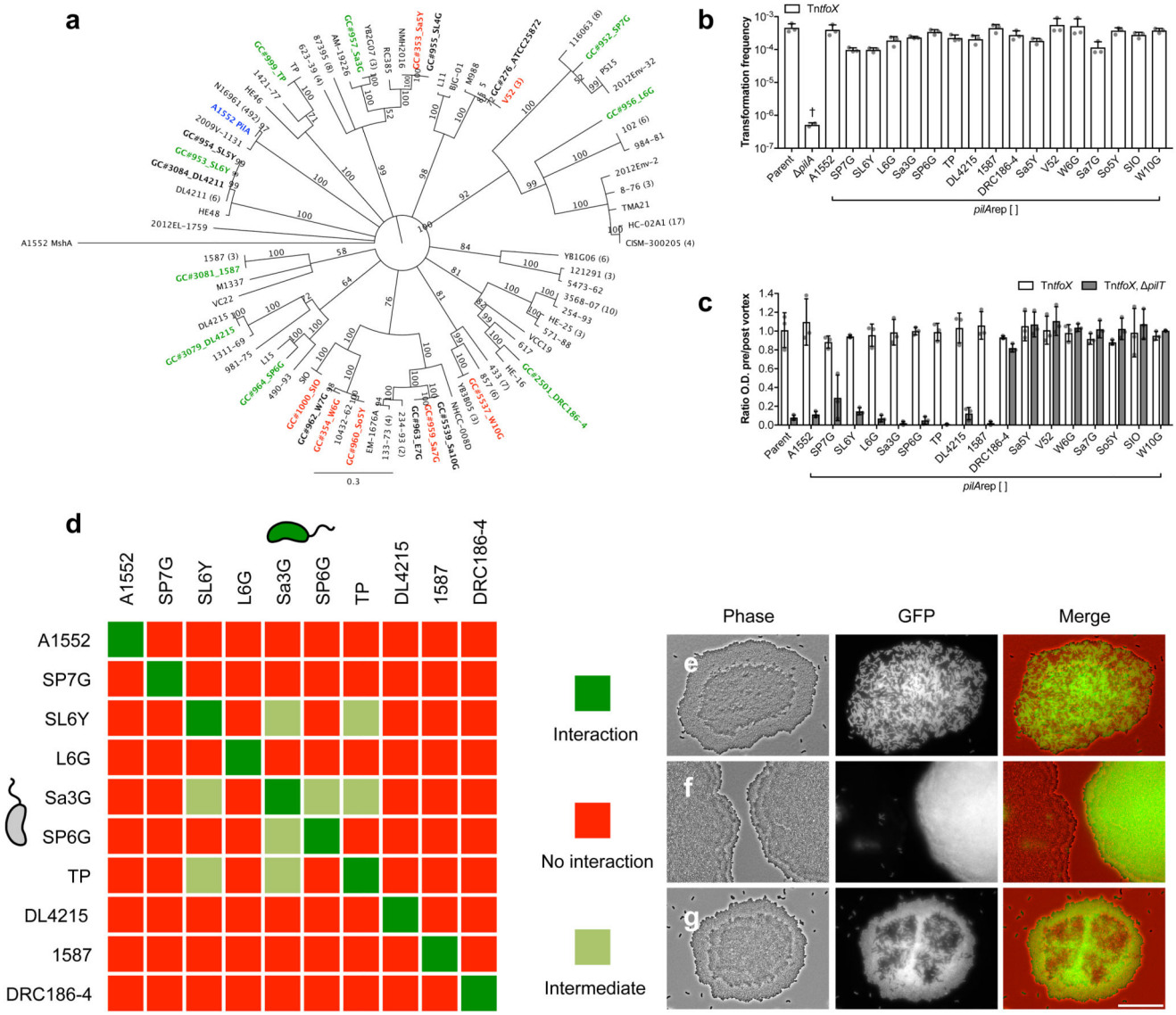

Figure 4. PilA variability governs auto-aggregation and enables kin-recognition.

(**A**) Consensus neighbour-joining phylogenetic tree of PilA. The tree consists of the 56 unique PilA sequences identified from NCBI, 22 sequences from an in-house collection of various environmental and patient isolates (bold), and A1552 PilA (blue) and MshA (outgroup). Values shown are consensus support values (%). Aggregation capable (green) and incapable (red) PilAs tested in the *pilA*rep experiments are highlighted. Note that ATCC25872 and V52 PilA are identical.

(**B**-**C**) Functionality of A1552-Tn*tfoX*, *pilA*rep[A1552] and 16 different PilA variants assessed by transformation and aggregation. (**B**) Chitin-independent transformation frequency assay. WT parent (A1552-Tn*tfoX*) and Δ*pilA* (A1552-Tn*tfoX*, Δ*pilA*) strains served as positive and negative controls. Transformation frequencies are the mean of three repeats (+S.D.). †, <d.l. in one repeat. (**C**) Aggregation was determined for the WT parent and each *pilA*rep strain in a *pilT*+ (A1552-Tn*tfoX*) and Δ*pilT* (A1552-Tn*tfoX*, Δ*pilT*)

Europe PMC Funders Author Manuscripts

background, as indicated. Aggregation is shown as the ratio of the culture optical density (O.D. $_{600}$) before and after vortexing, in the presence of *tfoX* induction. Values are the mean of three repeats (±S.D.).

(**D**) Interaction matrix showing the results of a pairwise analysis of all possible interactions between aggregation-proficient PilA variants. Interactions were tested by co-culturing non-fluorescent cells of the relevant Tn*tfoX*, Δ*pilT*, pilA*rep*[XX] strains with a fluorescent (GFP +) derivative of each strain. Cells were grown in the presence of *tfoX* induction. Self-self combinations served as controls.

(**E-G**) Representative examples of (**E**) interaction, resulting in well-mixed aggregates (**F**) no interaction, resulting in fluorescent or non-fluorescent aggregates and (**G**) intermediate interactions, resulting in patterned aggregates. Merged images show GFP in green and phase-contrast (Phase) in red. Bar = 25 μm.

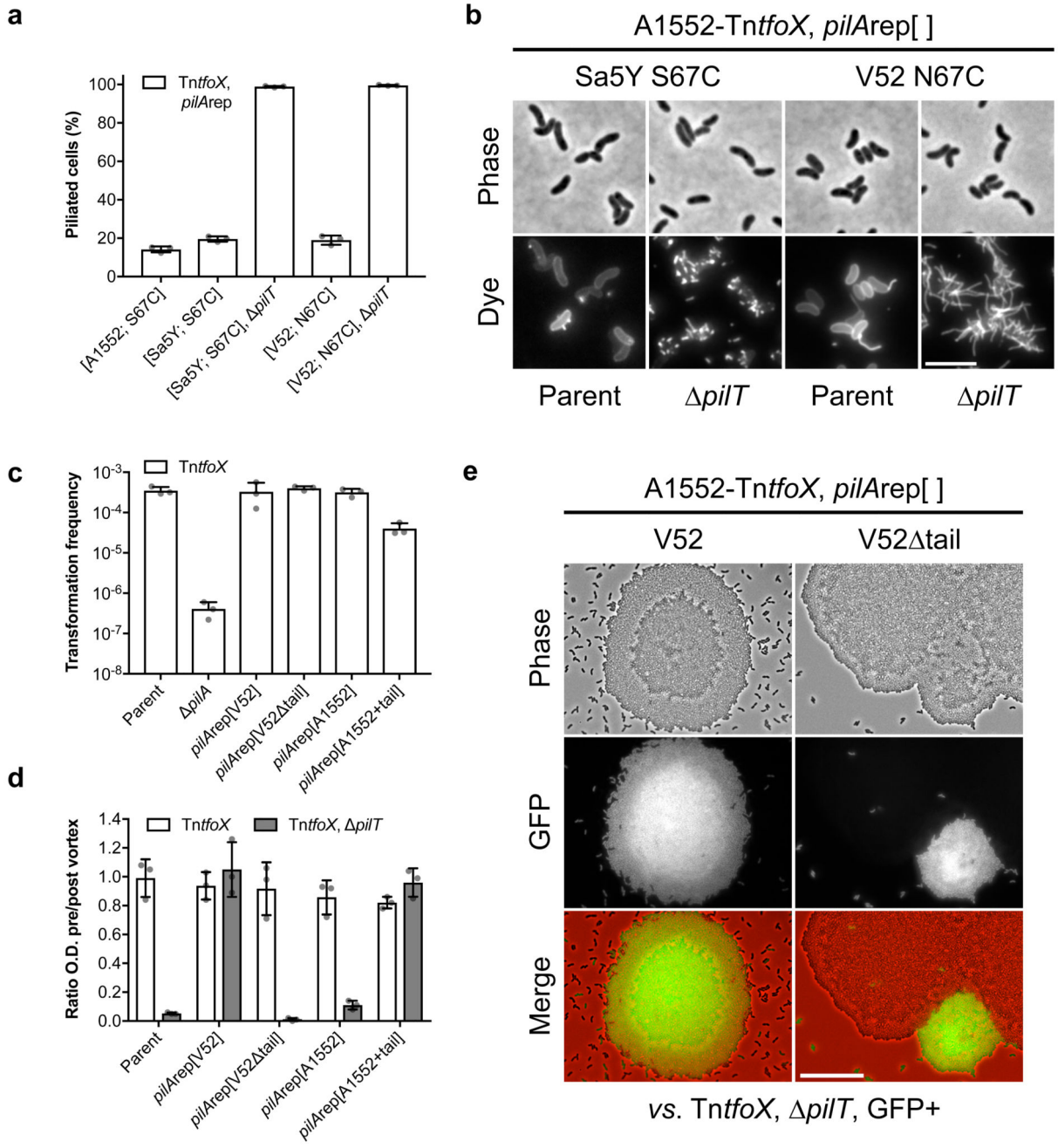

Figure 5. The unusual tail of ATCC25872/V52 PilA inhibits aggregation.

(**A**) Quantification of piliation in snapshot imaging of cells of strains A1552-Tn*tfoX*, *pilA*rep[A1552; S67C], A1552-Tn*tfoX*, *pilA*rep[Sa5Y; S67C] and A1552-Tn*tfoX*, *pilA*rep[V52; N67C], in the indicated backgrounds. Cells were grown with *tfoX* induction and pili stained with AF-488-Mal. Bars represent the mean of three repeats (±S.D.). n = *c.a.* 2000 cells per strain per repeat. (**B**) Direct observation of pili stained with AF-488-Mal in cells carrying *pilA*rep[Sa5Y; S67C] and *pilA*rep[V52; N67C], in a WT parent (A1552-Tn*tfoX*) and Δ*pilT* (A1552-Tn*tfoX*, Δ*pilT*) background, as indicated. Bar = 5 μm.

Europe PMC Funders Author Manuscripts

(**C**-**D**) Functionality of *pilA*rep tail variants assessed by natural transformation and aggregation. (**C**) Chitin-independent transformation assay. WT parent (A1552-Tn*tfoX*) and Δ*pilA* (A1552-Tn*tfoX*, Δ*pilA*) strains served as positive and negative controls. Transformation frequencies are the mean of three repeats (+S.D.). (**D**) Aggregation was determined for the WT parent and each *pilA*rep strain in a *pilT*+ (A1552-Tn*tfoX*) and Δ*pilT* (A1552-Tn*tfoX*, Δ*pilT*) background, as indicated. Aggregation is shown as the ratio of the culture optical density ($O.D._{600}$) before and after vortexing, in the presence of *tfoX* induction. Values are the mean of three repeats (±S.D.).
(**E**) Co-culture of fluorescent cells of A1552-Tn*tfoX*, Δ*pilT*, GFP+, producing GFP, and non-fluorescent cells of either *pilA*rep[V52] (A1552-Tn*tfoX*, Δ*pilT*, *pilA*rep[V52]) or *pilA*rep[V52Δtail] (A1552-Tn*tfoX*, Δ*pilT*, *pilA*rep[V52Δtail]), as indicated. Note that ATCC25872 and V52 PilA are identical. Cells were grown in the presence of *tfoX* induction. Merged images show GFP in green and phase-contrast in red. Bar = 25 μm.

Europe PMC Funders Author Manuscripts

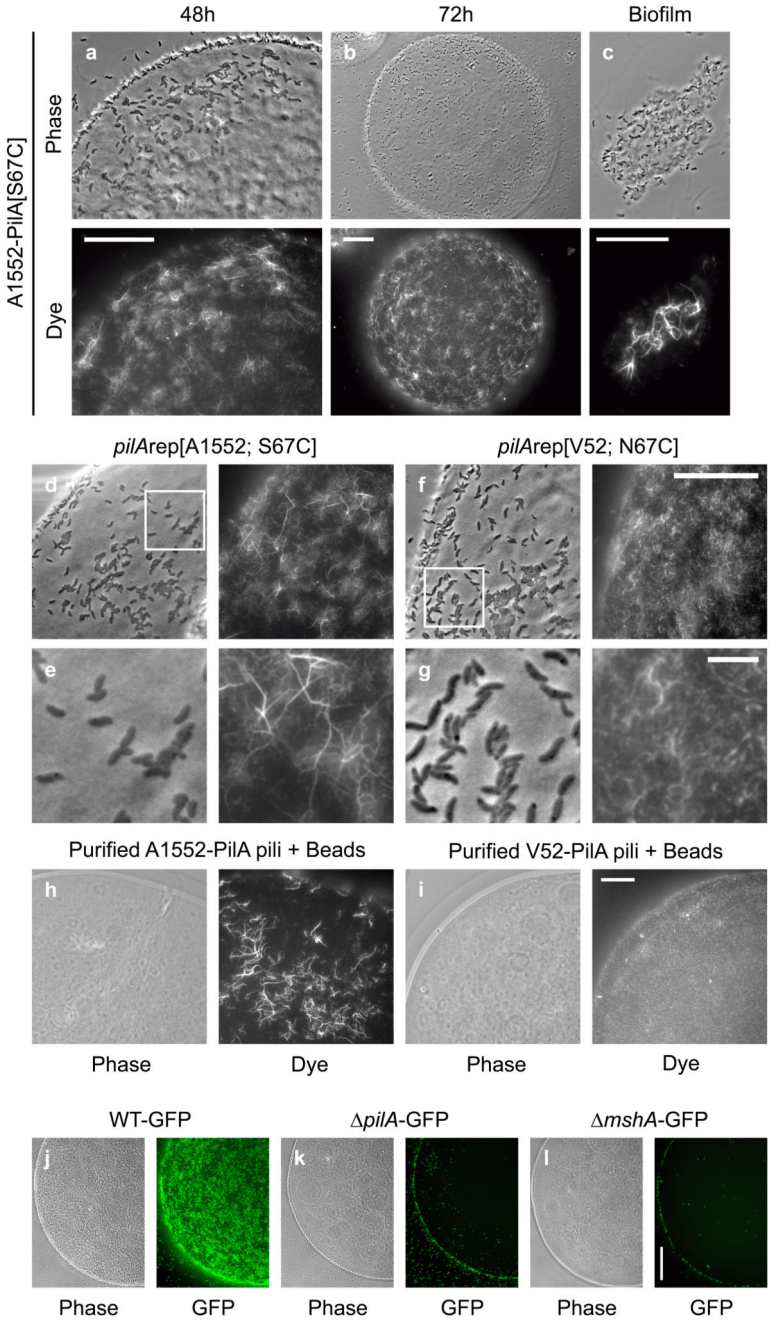

Figure 6. DNA-uptake pili form networks on chitin surfaces.

(**A**-**C**) DNA-uptake pili composed of A1552-PilA form networks naturally on chitin surfaces. Chitin beads were stained with AF-488-Mal after incubation for either 48h (**A**) or 72h (**B** and **C**) in defined artificial seawater (DASW) with cells of A1552-PilA[S67C], as indicated. Panel (**C**) depicts a piece of detached biofilm-like material; note the retention of the pilus networks. Bars = 25 μm.

(**D**-**G**) The ability to form pilus networks is dependent on the ability to self-interact. Chitin beads were stained with AF-488-Mal after incubation for 48h in DASW with cells of either

(**D**) A1552-*pilA*rep[A1552; S67C] or (**F**) A1552-*pilA*rep[V52; N67C], as indicated. Panels (**E** and **G**) show enlargements of the boxed regions of the surfaces shown in (**D** and **F**). Note the absence of large pili networks in (**G**). Bars = 25 μm (D, F) and 5 μm (E, G).

(**H**-**I**) DNA-uptake pili bind to chitin surfaces. Chitin beads were stained with AF-488-Mal after incubation for 1h with purified DNA-uptake pili composed of either (**H**) A1552-PilA; [S67C] or (**I**) V52-PilA; [N67C], as indicated. Bar = 25 μm.

(**J**-**L**) DNA-uptake pili are required for chitin colonisation under flow. Chitin beads were imaged after incubation in DASW for 48h under conditions of continuous mixing with GFP + cells of strains (**J**) A1552-GFP (WT-GFP), (**K**) A1552-GFP, Δ*pilA* (Δ*pilA*-GFP) and (**L**) A1552-GFP, Δ*mshA* (Δ*mshA*-GFP), as indicated. Bar = 50 μm.